Impurity-induced spin pseudogap in $SrCuO_2$ doped with Mg, Zn, or La

Dalila Bounoua,[1] Romuald Saint-Martin,[1] Sylvain Petit,[2] Patrick Berthet,[1] Françoise Damay,[2] Yvan Sidis,[2] Frédéric Bourdarot,[3] and Loreynne Pinsard-Gaudart[1]

[1]*Equipe Synthèse Propriétés et Modélisation des Matériaux, Institut de Chimie Moléculaire et des Matériaux d'Orsay, Centre National de la Recherche Scientifique UMR 8182, Université Paris-Sud, Université Paris-Saclay, 91405 Orsay, France*

[2]*Laboratoire Léon Brillouin, Commissariat à l'énergie atomique et aux énergies alternatives (CEA), Centre National de la Recherche Scientifique (CNRS), Université Paris-Saclay, F-91191 Gif sur Yvette, France*

[3]*Institut Nanosciences et Cryogénie (INAC)–Service de Physique Statistique Magnétisme et Supraconductivité (SPMS), CEA and Université Joseph Fourier, F-38000 Grenoble, France*

(Received 6 March 2017; published 26 June 2017)

The low energy magnetic excitations spectra of the pristine and doped quasi-one-dimensional spin chains cuprates $SrCuO_2$ have been investigated by inelastic neutron scattering. The momentum-integrated magnetic dynamical structure factor yields a constant integrated intensity with regard to energy in the pure compound, while it shows a strong decay, at low energies, in the compounds doped with nonmagnetic impurities, namely, $SrCu_{0.99}M_{0.01}O_2$ (with M = Zn or Mg) and $Sr_{0.99}La_{0.01}CuO_2$ (Cu^+ carrying $S = 0$ created within the chains). These results evidence the opening of a spin pseudogap in the two-spinon continuum of $SrCuO_2$ upon doping, stemming from disruptions of the spin chains by quantum impurities.

DOI: 10.1103/PhysRevB.95.224429

I. INTRODUCTION

Quasi-one-dimensional (1D) copper oxides, such as Mott insulating $SrCuO_2$ and Sr_2CuO_3, are known to exhibit anisotropic ballistic heat transport [1]. Despite the absence of any electronic contribution to heat conduction (κ), the amplitude of κ along the Cu-O chains remains strikingly high, namely, $\kappa \sim 800\,W\,K^{-1}\,m^{-1}$ and $500\,W\,K^{-1}m^{-1}$ at 27 and 22 K in $SrCuO_2$ and Sr_2CuO_3 [1–4], respectively. Thermal transport along the chains is controlled by lattice and spin degrees of freedom and their related quasiparticles: phonons and spinon. The mean free paths of both types of quasiparticles turn out to be highly sensitive to two-particle and particle-defect scattering processes. Substitution by magnetic or nonmagnetic quantum impurities, on the copper site, allows the investigation of the spinon-defects scattering mechanism and determining whether the chains "heal" the defects or whether the defects sever the chains.

$SrCuO_2$ crystallizes in the orthorhombic space group *Cmcm*. The spin chains are formed by the alternating Cu-O-Cu ions, arranged along the c-crystallographic direction, with $\sim 177^\circ$ bonding angle. Cu^{2+} ions are square-planar coordinated, thus carrying spin 1/2, and are organized in corner sharing CuO_4 units [5]. Along the c axis, two parallel spin chains are found, distanced by one Cu-O bond length, thus resulting in the so-called zigzag chain of Cu^{2+} ions (Fig. 1). The intrachain antiferromagnetic superexchange coupling is $J_{AFM} \sim 2000$ K, while the interchain ferromagnetic superexchange coupling, through the $\sim 93^\circ$ oxygen bridge, is frustrated with $J_{FM} \sim 200$ K [6–10] (Fig. 1). The two chains are hence very weakly coupled, and the material is described as a quasi-1D spin chains system rather than a two legs ladder one. $SrCuO_2$ undergoes, on cooling, a magnetic transition at $T_N < 2$ K from a 1D regime, where only next neighbors interactions within the spin chains subsist with no long-range ordering, to an incommensurate antiferromagnetic long-range order [10,11].

$SrCuO_2$ is usually described as an experimental realization of the uniform XXZ Heisenberg model [7,12]:

$$H = J \sum_n \left\{ \frac{1}{2}(S_n^+ S_{n+1}^- + S_n^- S_{n+1}^+) + \Delta S_n^z S_{n+1}^z \right\}.$$

These systems are also referred to as quantum critical Tomonaga-Luttinger spin liquids [13–15]. The ground state, with the anisotropy parameter $\Delta = 1$, is found to be gapless, while its magnetic excitations spectrum is described by the famous Des Cloiseaux-Pearson two-spinon continuum [16,17]. Substitution on the Cu^{2+} site shows that a minute amount of quantum impurities gives rise to unexpected behaviors: A spin pseudogap opens in the des Cloiseaux–Pearson two-spinon continuum [18–22], arising from chains fragmentation into finite length segments. The spin gap, denoted Δ_L, scales with the amount of impurities as $\Delta_L = \frac{\Delta_0}{L}$, where $\Delta_0 = 3.65\ J_{AFM}$ [23] is a typical gap and L is the chain length of the created segments, i.e., the distance between two subsequent impurities, averaged to $L \sim \frac{1}{x}$, where x is the amount of dopant.

In this paper, we propose a comparison between the low energy spectra of the pristine $SrCuO_2$ and the $S = 0$ doped $SrCu_{0.99}M_{0.01}O_2$ (M = Zn or Mg) and $Sr_{0.99}La_{0.01}CuO_2$. This last doping is expected to induce Cu^+ within the chains.

We aim at extracting a general trend of the doping effect to further link it to results from transport measurements. To this end, inelastic neutron scattering (INS) measurements have been conducted on our materials. We determine the doping impact on the magnetic excitations spectra of all the compounds. Meanwhile, neutron diffraction experiments have been performed on samples of the same compositions in order to confirm that no magnetic transition occurs in the temperature range of interest and hence to ensure that the INS have been carried out in the 1D regime.

II. CRYSTAL GROWTH AND CHARACTERIZATION

All INS experiments were performed on high-quality single crystals grown by the traveling solvent floating zone method.

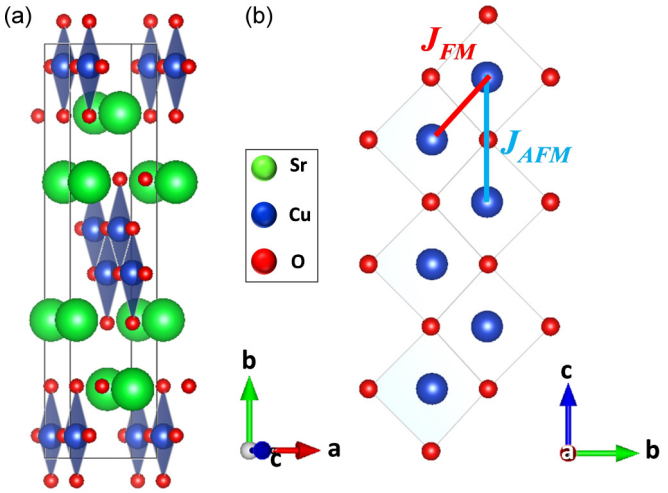

FIG. 1. (a) Crystal structure of $SrCuO_2$. (b) Projection on the *bc* plane of the structure that shows the zigzag chains of Cu^{2+} ions. J_{AFM} and J_{FM} refer to the coupling constants of the antiferromagnetic and ferromagnetic superexchange interactions in the chains, respectively, as described in the text.

The crystal growth has been realized from polycrystalline powders of the orthorhombic $SrCuO_2$ and the corresponding doped compounds. The phase $SrCuO_2$ has been synthesized through solid state reaction by mixing the following precursors in stoichiometric proportions: $SrCO_3$ (99.99%), CuO (99.99%); for the dopant: La_2O_3 (99.995%), ZnO (99.99%), and MgO (99.95%). After three long heat treatments at 920, 960, and 980°C for 24, 48, and 48 hours, respectively, and intermediate grindings, feed rods of the materials have been prepared by packing the powders inside latex tubes of 7 mm diameter. The powders were then compacted using an isostatic pressure setup under 2200 bars, and the resulting feed rods sintered at 980°C for 48 h prior to the growth.

The single crystal growth has been conducted in a four mirrors image furnace (Model CSI FZ-T-10000-H-VII-VPO-PC, Crystal System Corporation Company). $SrCuO_2$ being an incongruently melting compound, the solvent zone has been initiated by melting a cupric oxide (CuO) pellet at the beginning of the growth for all the compounds, except for the case of Zn-doped $SrCuO_2$ where 1% of Zn has been added to the CuO pellet. Indeed, we have found that during the crystal growth, the Zn^{2+} was accumulated in the solvent zone (of initial composition CuO). Consequently, elemental analysis investigations revealed that the level of dopant in the final crystal was significantly lower than 1%. However, while starting the growth with a solvent zone already containing the Zn precursor, namely (99%CuO−1%ZnO), it comes out that the concentration of the impurity in the single crystal is much closer to the wanted amount. The growth has been performed at a rate of 1 mm/h under O_2 flux (75 mL/min).

All the rods of doped $SrCuO_2$ contained the same initial amount of dopant, namely, 1% of Zn^{2+},Mg^{2+}, or La^{3+}. The quantity of the dopant in the grown single crystals has been checked out systematically by elemental analysis techniques, that is, x-ray photoelectron spectroscopy or energy dispersive x-ray spectroscopy. The elemental analysis revealed good agreement with the nominal values of 1%.

The magnetic susceptibilities of the single crystals have been measured along the spin chains direction (*c* axis) using a superconducting quantum interference device ([SQUID] magnetometer, Quantum Design Magnetic Property Measurement System [MPMS]) under a magnetic field of 1000 Oe (see Appendix A). The fits to the curves, using the Bonner-Fischer expression [23–25] with logarithmic correction, allowed the determination of the Curie constants, Curie-Weiss temperatures, and the antiferromagnetic superexchange coupling constants J_{AFM}.

The results, given in Table I, point out an increase of the Curie constant in all of the doped $SrCuO_2$ compounds arising from the unpaired spins belonging to the odd number of spins-segments length generated upon cutting the chains by the substituent. A slight decrease of J_{AFM} is also evidenced in the Zn− and La-doped $SrCuO_2$. These outcomes highlight the fact that the dopant is, indeed, incorporated within the spin chains and acts as a chains breaker.

Complementary neutron diffraction measurements were carried out on the cold neutron diffractometer G4.1 at the reactor ORPHÉE (CEA Saclay). The measurements were completed at 1.5, 2, 20, 28, 32, 37, 60, and 80 K in order to cross the temperature range where the thermal conduction peak emerges [2]. Data were collected at $2^\circ \leqslant 2\theta \leqslant 83^\circ$ with a step of 0.1° and a wavelength of 2.423 Å (see Appendix B). The measured powders were obtained by grinding parts of the grown single crystals ($SrCuO_2$, Mg-, and La-doped $SrCuO_2$). The powders have been poured into vanadium cylindrical sample holders and then introduced into the cryostat. Rietveld structural refinements have been achieved on the whole diffraction patterns using Fullprof software. A careful examination of the data reveals that the Bragg reflections display no evolution upon heating in terms of intensity or width, and no supplementary magnetic Bragg peaks were observed across the 2θ range of measurement over all the compositions. The structural refinement results evidence the absence of any structural or magnetic transition from $T = 1.5$ to 80 K, along

TABLE I. Resulting fit parameters to the magnetic susceptibility data, measured along the spins chains direction (*c* axis) for the pristine and (Mg − ,Zn−, or La)-doped $SrCuO_2$.

Compound	C (emu K^{-1} mol^{-1})	$\Theta_{cw}(K)$	X_0(emu/mol)	J_{AFM}(K)
$SrCuO_2$	3.1×10^{-5}	− 0.63	7.0×10^{-5}	2009 ± 200
$SrCu_{0,.99}Mg_{0.01}O_2$	3.2×10^{-4}	0.39	2.4×10^{-4}	1845 ± 200
$SrCu_{0.99}Zn_{0.01}O_2$	7.4×10^{-5}	− 0.63	2.4×10^{-4}	1801 ± 200
$La_{0.01}Sr_{0.99}CuO_2$	2.4×10^{-4}	− 0.74	2.6×10^{-5}	1803 ± 200

with no significant evolution of the unit cell parameters with regard to temperature.

On the other hand, specific heat measurements on an as grown single crystal of $SrCuO_2$ show that the long-range magnetic order starts to take place only at $T_N \approx 1.7$ K. It should be mentioned here that the Néel transition displacement towards lower temperatures is expected in the doped samples. Indeed, it has been demonstrated [26] that even very low amounts of Ni impurities (less than 1%) could disturb the magnetic ordering or further suppress it in the ($x = 0.5\%$ or more) Ni-doped $SrCuO_2$. It is well established that Ni^{2+} ions in $SrCuO_2$ act as nonmagnetic impurities ($S = 0$), as square planar coordinated $3d^8$ ions take their low-spin state [27,28]. This brings us to a comparable situation as doping with nonmagnetic Mg, Zn, or La (La-induced $S = 0$ impurities). The same behavior can, then, similarly be expected, i.e., the impurities prevent the long-range order from establishing moving T_N to temperatures lower than 1.7 K.

III. SPIN DYNAMICS

The INS studies were carried out on triple axis spectrometers (TAS): thermal TAS IN22 (CEA–Collaborative Research Group Beamline) located at Institut Laue-Langevin (ILL), thermal TAS 2T1, and cold TAS 4F1 and 4F2 at reactor ORPHÉE (CEA Saclay). All the spectrometers were equipped with focusing Pyrolitic Graphite (PG) 002 monochromators and analyzers. A PG filter was implemented in the scattered beam to remove high order contamination. The final energy E_f was set to 14.7 meV or 9.5 meV. The INS measurements were performed on four large single crystals: pure $SrCuO_2$ (weight 1.5 g, $T = 4$ K on IN22), $SrCu_{0.99}Mg_{0.01}O_2$ (weight 1.8 g, $T = 4$ K on 2T1 and $T = 1.5$ K, 40 and 100 K on 4F1), $SrCu_{0.99}Zn_{0.01}O_2$ (weight 1.0 g, $T = 6$ K on 4F2), and $Sr_{0.99}La_{0.01}CuO_2$ (weight 1.2 g, $T = 1.5$ K on 4F1).

The samples were mounted on the cold finger of a closed circle refrigerator or a standard orange cryostat. The samples were aligned in the $[h, 0, l]$ scattering plane. Hereafter, wave vectors are given in reduced lattice units (r.l.u.) $2\pi/a = 1.76$ Å^{-1} and $2\pi/c = 1.61$ Å^{-1}, with $a = 3.57$ Å and $c = 3.91$ Å.

Following neutron diffraction results, the INS experiments have been realized in the 1D regime, above any long-range ordering temperature ($T > T_N$) so that the emerging magnetic signal could be, unambiguously, ascribed to the two-spinon spectrum that is expected to appear at $l = 0.5$ [13]. As the system is purely 1D, down to the ordering temperature, the spin excitations spectrum is expected to be h independent; h was set to 1. (Note that as h goes to 0, the intrinsic nonmagnetic background increases as one approaches the direct beam.) The study was further restricted to the energy range $0.5 \leqslant \hbar\omega \leqslant 10$ meV because above 12 meV, the magnetic signal starts overlapping with optical phonons modes, making the tracking of the magnetic contribution harder.

Figure 2(a) shows an energy-momentum map of the neutron scattering intensity in $SrCu_{0.99}Mg_{0.01}O_2$ at $T = 1.5$ K in the 1D regime. As shown by the constant energy scans in Fig. 2(b), a magnetic signal appears at $l = 0.5$ on top of a featureless background. This magnetic signal displays a Gaussian profile with decreasing intensity when decreasing the transfer energy.

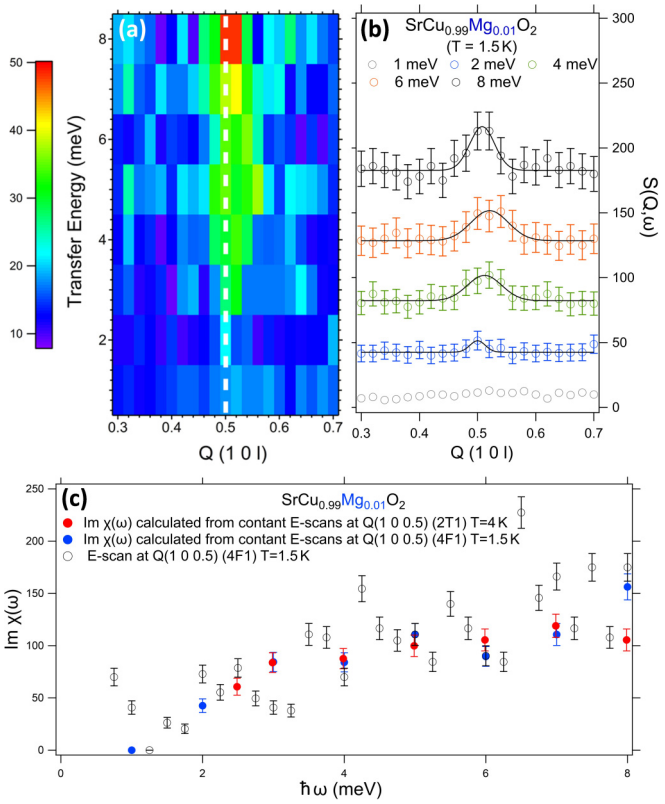

FIG. 2. (a) Typical (Q, ω) color map of the low energy magnetic excitations spectrum obtained by INS in the Mg-doped $SrCuO_2$. The white dashed line shows the center of the spin excitations spectrum. (b) Constant energy scans following the trajectory $Q\,(1\,0\,l)$ with $l = [0.3-0.7]$ at $T = 1.5$ K, on the TAS 4F1. (c) Comparison of the imaginary part of the dynamical magnetic susceptibility obtained by fits to the constant E scans on the TAS 4F1 (1.5 K) and 2T1 (4 K) and the energy scan at $Q(1\,0\,0.5)$ on the TAS 4F1 (1.5 K).

In order to reveal the energy dependence of the magnetic scattering, the background has been estimated from the constant energy scans at l values away from $l = 0.5$, where no magnetic signal is expected, namely, $l = 0.3$ and $l = 0.7$. A polynomial fit to the background points has been realized for each set of data, Q (1 0 0.3) and Q (1 0 0.7), and then subtracted from the constant momentum scan at Q (1 0 0.5). The magnetic signal is proportional to the spin-spin correlation function,

$$S(Q,\omega) = [1 + n_B(\omega,T)]\,\mathrm{Im}\,\chi(Q,\omega), \qquad (1)$$

where Im $\chi(Q,\omega)$ stands for the imaginary part of the dynamical magnetic susceptibility and $[1 + n_B(\omega,T)]$ corresponds to the detailed balance factor.

Figure 2(c) shows the energy dependence of Im $\chi(Q,\omega)$, as derived from the aforementioned experimental procedure. Results show a depletion of the density of states in the low energy region of the magnetic excitations spectrum of the compound, a signature of the opening of a spin pseudogap.

The same experimental procedure was systematically used for the study of the pristine and the 1%-substituted (Mg, Zn, or La) $SrCuO_2$ samples (see Appendix C). At variance with the pure system [Fig. 3(a)], the q-integrated (or local)

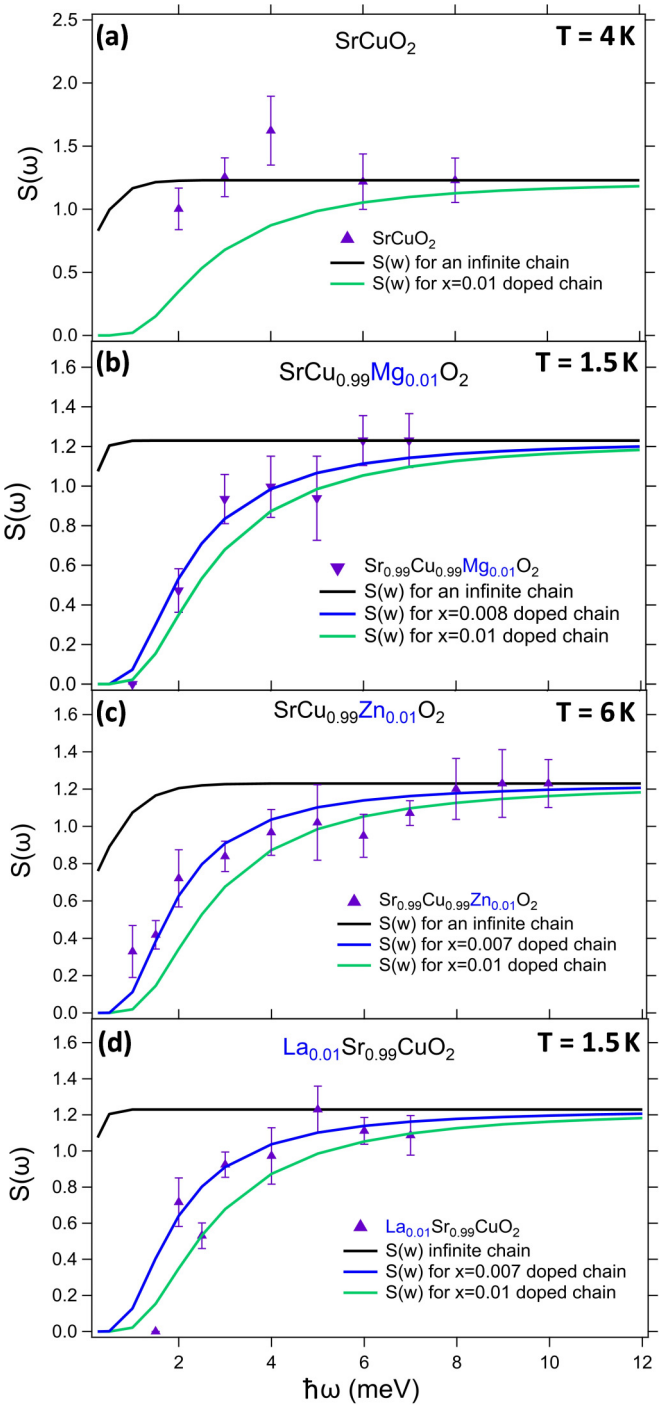

FIG. 3. (a)–(d) Comparison of the measured dynamical structure factors for the pristine Mg − ,Zn−, and La− doped $SrCuO_2$ (violet triangles), respectively, with the theoretical $S(\omega)$ for an infinite chain (black line) and for a 1 and x%-doped chain (green and blue lines, respectively).

spin-spin correlation function $S(\omega)$ systematically exhibits a spin pseudogap in the substituted materials [Figs. 3(b)–3(d)].

IV. DISCUSSION

The formation of a pseudogap in the magnetic excitations spectrum of the doped $SrCuO_2$ compounds is induced by the presence of the nonmagnetic ($S = 0$) defects: Mg^{2+},Zn^{2+}, and Cu^{+} ions. The quantum impurities cause local disruptions of the spin chains, thus breaking the interaction path between two neighboring copper ions and dividing the chains into finite length segments. This results in a chain lengths distribution and leads to a decay of the spin-spin correlation lengths. Due to the finite size effect, a depletion of the density of states in the low energy region of the spectrum follows. A distribution of spin gaps with values that scale with the chains lengths as $\frac{1}{L}$ (with L being the chain length) develop, and the sum over all the possible segments lengths yields the pseudogap. In other words, $S = 0$ point defects act as barrier walls that scatter the spinon, and as the system is 1D, the consequences are important and result in a gaped two-spinon continuum.

Note that Karmakar *et al.* [19] reported that the spin excitations spectrum of the 2% Zn-doped $SrCuO_2$ was gapless. The most likely reason for the discrepancy between both results is that the effective amount of Zn^{2+} in their final grown crystal was significantly lower than the nominal doping level of 2%, probably due to the different starting conditions of crystal growth (cf. Sec. II). Therefore, as the spin pseudogap is found to scale with x, which is the amount of impurities within the chains, this feature could not be evidenced in Ref. [19].

In order to determine the amount of impurities "seen" by spinon, an attempt has been made to fit the momentum integrated dynamical structure factors of each compound with the model proposed by Simutis *et al.* [18].

Consider the momentum-integrated dynamical structure factor of a spin chain of infinite length, described as follows [18]:

$$S_\infty(\omega) = (\gamma r_0)^2 \frac{k_f}{k_i} \frac{2g^2}{4} A \frac{n_B(\omega)+1}{\pi J_{\mathrm{AFM}}} \tanh\left(\frac{\hbar\omega}{2k_B T}\right), \quad (2)$$

where $(\gamma r_0)^2 = 0.290$ barn, k_i and k_f are the incident and final wave vectors, respectively, $A = 1.34$ is the Müller Ansatz normalization [29], and $g = 2.12$ is the average gyromagnetic ratio for the copper spin within the chains [30].

Equation (2) can be expressed for a finite length chain as [18]:

$$S(\omega) = S_\infty(\omega) F_{\Delta_L}(\omega) \quad (3)$$

$$F_{\Delta_L}(\omega) = \left(\frac{\Delta_L}{2\hbar\omega}\right)^2 \sinh^{-2}\left(\frac{\Delta_L}{2\hbar\omega}\right), \quad (4)$$

where Δ_L corresponds to the pseudogap and is estimated to be equal to $\Delta_L = x\,\Delta_0$ and $F_{\Delta_L}(\omega)$ is the envelope function that takes into account the distribution of chain segments lengths.

The $S(\omega)$ curves in Fig. 3 have been normalized by a scaling factor and compared to the theoretical structure factors of an infinite and x-doped chains. The momentum integrated dynamical structure factor, for the pristine $SrCuO_2$, shows nice agreement with the theoretical curve of an infinite chain length, while those of the doped compounds overlap

with the calculated $S(\omega)$ from Eq. (4) for $x = (0.80 \pm 0.06)$, (0.68 ± 0.051), and $(0.83 \pm 0.08)\%$ upon Mg, Zn, and La doping, respectively.

The results reveal an underestimated value of the nominal amount of dopant, which might be due to a distribution of the impurity concentration during the crystal growth. However, for the case of Mg doping, another possible reason for the difference between thenominal and estimated dopant amount is that some of the Mg^{2+} might not substitute the Cu^{2+} site but rather go on the Sr^{2+} site. This can explain the previous result, as the measured spectra probe only the signal coming from the chains, leaving the out-chains impurities undetected.

The sizes of the pseudogaps are estimated from fits to the momentum-integrated dynamical structure factors $S(\omega)$ by Eq. (4). The resulting values for Δ_L are 6.6 ± 0.5,5.5 ± 0.4, and 6.8 ± 0.7 meV upon Mg, Zn, and La doping, respectively.

The pseudogap in the Mg-doped compound mainly arises from the $S = 0$ scattering centers introduced within the chains. Additionally, if some of the Mg^{2+}, indeed, substitutes the Sr^{2+} site, it would locally induce bond distortions in the neighboring Cu-O-Cu chains that might contribute to the opening of the pseudogap. In fact, it has been demonstrated that doping, even outside the chains, with Ca^{2+} ions, results in gaped magnetic excitations spectra for $Sr_{0.9}Ca_{0.1}CuO_2$ (5 meV) and its parent compound $Sr_{1.9}Ca_{0.1}CuO_3$ (9 meV). Due to the different ionic radii of Sr^{2+} (1.21 Å) and Ca^{2+} (1.06 Å), the spin chains are affected by changes of the Cu-O-Cu bonding angles, which locally alter or break the antiferromagnetic superexchange coupling. Such bond disorder is enough for the occurrence of a spin pseudogap [20–22]. However, given the amount of Mg^{2+} that might go on the Sr^{2+} site in the 1% Mg-doped $SrCuO_2$, its impact on the low energy region of the two spinon continuum is expected to be very slight.

The situation is the same upon La doping. The origin of the gap is the creation of Cu^{+} ions, with $S = 0$, within the chains. Cu^{+} has an ionic radius of (0.60 Å), comparable to that of Zn^{2+}, and both the substituent impact the chains in the same manner. In this case, also, the presence of La^{3+} outside the chains can contribute to the depletion of the density of states at low energies, stemming from the different ionic radii of La^{3+} (1.10 Å) and Sr^{2+} (1.21 Å). But again, as the amount of La^{3+} ions located off the chains is low, the main reason for the opening of the spin pseudogap is the chains fractionalization by nonmagnetic punctual defects.

Moreover, to get an overview of the spin dynamics, one has further to crosscheck that the universal logarithmic $\hbar\omega/k_BT$ scaling of the q-integrated dynamical structure factor predicted for quantum critical Tomonaga-Luttinger spin liquids (TLL) [14,31] is fulfilled. To this end, measurements of the dynamical structure factor $S(\omega)$ at Q (1 0 0.5) have been carried out for $SrCu_{0.99}Mg_{0.01}O_2$ at several temperatures, namely, $T = 1.5$,4,40, and 100 K. The universal scaling feature of the dynamical correlations is independent of the microscopic properties of the system. Therefore, it should be insensitive to point defects such as the fractional amounts of $S = 0$ quantum impurities, as it is governed by quantum fluctuations. However, as reported previously [18], the opening of the spin pseudogap is known to induce a breakdown of the $\hbar\omega/k_BT$ scaling, given in Eq. (2). In order to recover that scaling behavior, one further needs to take into account the envelope function $F_\Delta(\omega)$, given by Eq. (4).

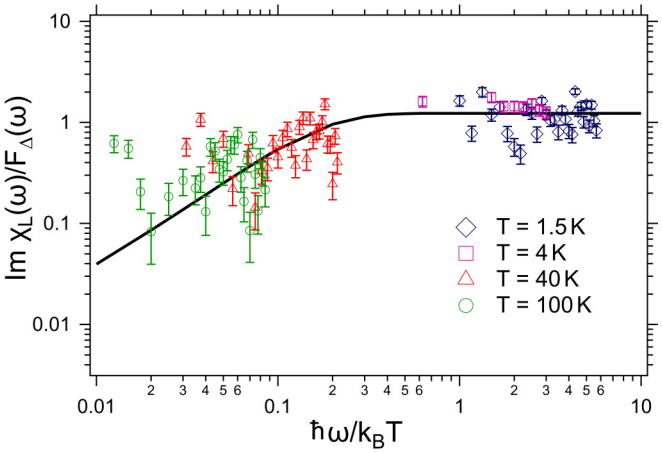

FIG. 4. Log-log plot of the evolution of Im $\chi_L(\omega)/F_\Delta(\omega)$ versus $\hbar\omega/k_bT$. Data collected at 1.5, 4, 40, and 100 K for $SrCu_{0.99}Mg_{0.01}O_2$ after normalization by the envelope function $F_\Delta(\omega)$ [Eq. (4)].

Figure 4 shows the universal ω/T scaling for the normalized imaginary part of the susceptibility Im $\chi_L(\omega)/F_\Delta(\omega)$. The envelope function is taken for a 0.8% Mg-doped $SrCuO_2$, as deduced from the fit to the dynamical structure factor of Mg-doped $SrCuO_2$ [Fig. 2(b)]. The low-energy/high-temperature cutoff in Im $\chi_L(\omega)/F_\Delta(\omega)$ (Fig. 4) arises from the occurrence of the spin pseudogap. However, for a given $\hbar\omega$, as the temperature increases, the spectral weight is shifted to higher energies, resulting in a displacement of the cutoff in Im $\chi_L(\omega)/F_\Delta(\omega)$ towards lower energies, and the pseudogap starts to be filled as the density of states within it increases.

This result might stand for an additional fact, supporting the universality of the envelope function proposed by Simutis *et al.* [18].

V. CONCLUSION

In summary, our work emphasizes a general trend (see also Refs. [18] and [22]), suggesting that the spin pseudogap opening is a common feature to all of the $S = 0$ substituted half integer spin chains cuprates, $SrCuO_2$ and Sr_2CuO_3, as a response to the finite size effect. An interesting issue would be to probe the impact of Mg and Zn doping in the parent single chain compound Sr_2CuO_3.

ACKNOWLEDGMENTS

This work has been supported by a grant from Domaine d'Intérêt Majeur du Réseau d'excellence francilien sur les Matériaux oxydes, Région Ile-de-France. Contract No. DO22RA14.

APPENDIX A: NEUTRON DIFFRACTION

Typical neutron diffraction patterns that were obtained on powdered $SrCuO_2$ are given in Fig. 5.

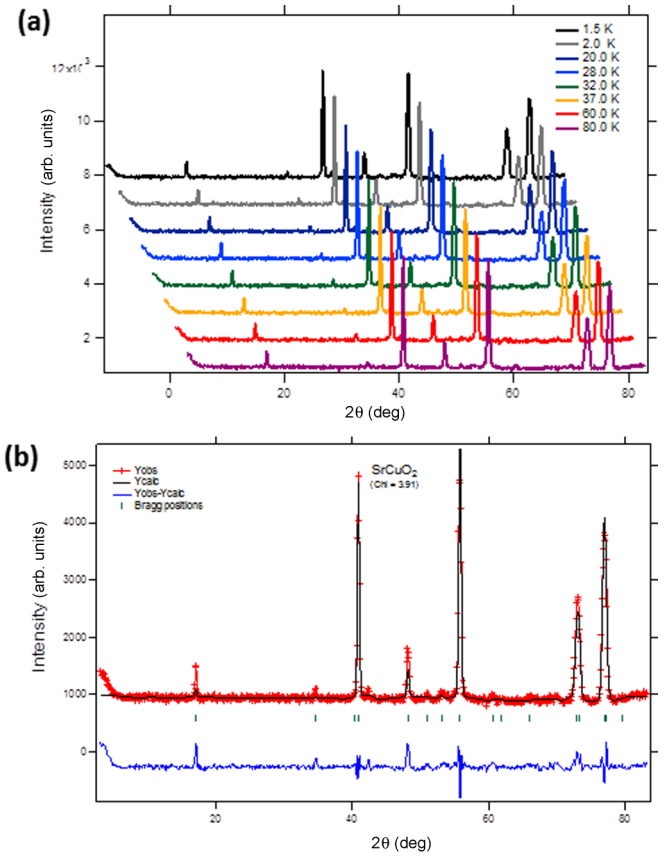

FIG. 5. (a) Neutron diffraction patterns of a grinded single crystal of $SrCuO_2$ at temperatures ranging from 1.5 to 80 K. (b) Typical structural Rietveld refinement result ($SrCuO_2$ at $T = 1.5$ K).

APPENDIX B: MAGNETIC SUSCEPTIBILITY

The magnetic susceptibility has been measured along the spin chains direction on single crystals of composition $SrCuO_2$ and Mg-, Zn-, or La-doped compounds. Results of the measurements are given in Fig. 6.

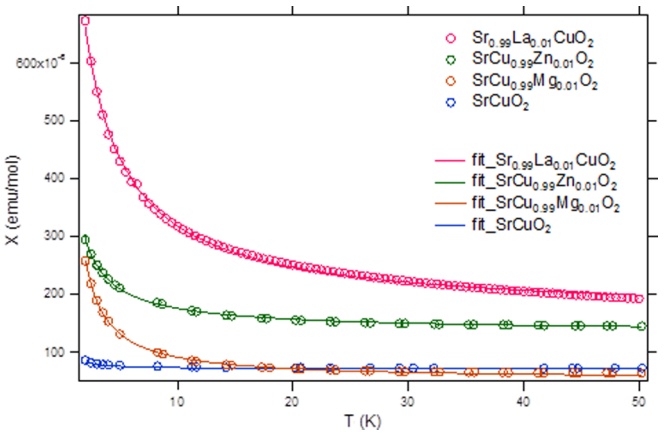

FIG. 6. Magnetic susceptibility measured along the spins chains (c axis) for the pristine Mg−,Zn−, and La− doped $SrCuO_2$ and their fits.

The fits have been realized following the equation:

$$\chi_{\text{Total}} = \chi_{\text{Curie}} + \chi_{\text{spin}} + \chi_0,$$

where χ_0 stands for a temperature-independent contribution, taking into account both Core diamagnetism and Van-Vleck paramagnetism; χ_{Curie} stands for Curie paramagnetic susceptibility expressed as $\chi_{\text{Curie}} = C/(T - \theta_{\text{CW}})$, where C and θ_{CW} are, respectively, the Curie constant and the Curie-Weiss temperature; and χ_{spin} arises from the magnetic susceptibility of the chains, expressed as

$$\chi_{\text{spin}} = n(g\mu_B)^2/(J\pi^2)(1 + 1/(2\ln(7.7/(k_B T)))),$$

where g, μ_B, and J are, respectively, the Landé factor for copper spin (set to $g = 2.21$), the Bohr magneton, and the superexchange coupling constant.

APPENDIX C: SPIN EXCITATIONS SPECTRA OF THE PRISTINE AND Zn- OR La-DOPED $SrCuO_2$

1. The pristine $SrCuO_2$

The constant energy scans obtained for the pristine $SrCuO_2$ show remaining intensity towards lower energies [Fig. 7(b)]. The magnetic excitations spectrum of the compound is given in terms of Im (χ) in Fig. 7(c).

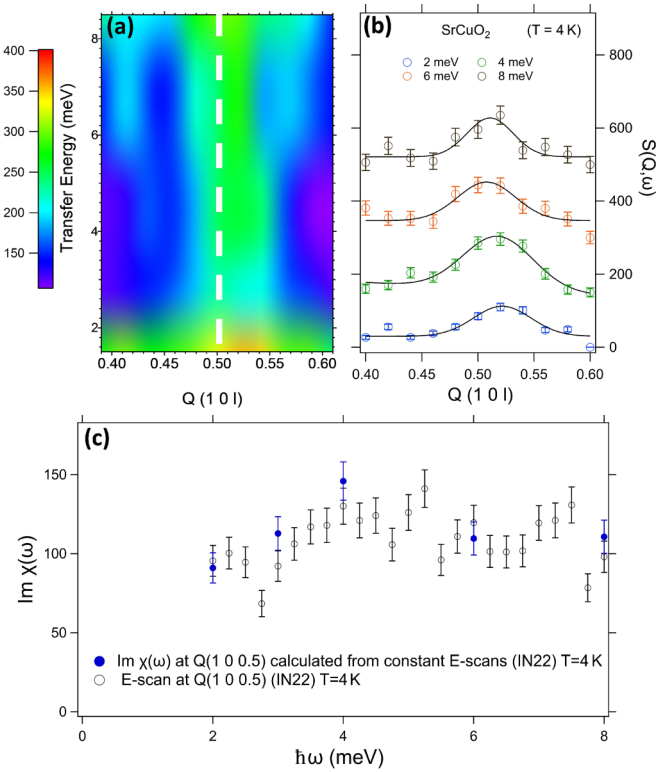

FIG. 7. (a) (Q, ω) color map of the low energy magnetic excitations spectrum obtained through INS in the pristine $SrCuO_2$; the white dashed line shows the center of the spin excitations spectrum. (b) Constant energy scans following the trajectory Q (1 0 l) with $l = [0.3-0.7]$ at $T = 4$ K on the TAS IN22. (c) Comparison of the imaginary part of the dynamical magnetic susceptibility obtained by fits to the constant E scans and the energy scan at Q(1 0 0.5).

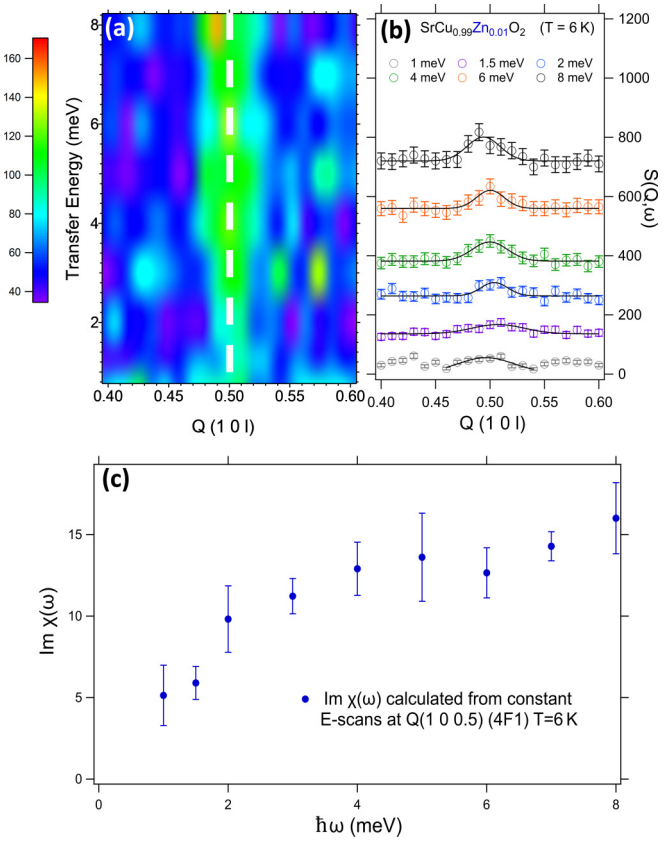

FIG. 8. (a) (Q, ω) color map of the low energy magnetic excitations spectrum obtained through INS in the Zn-doped $SrCuO_2$; the white dashed line shows the center of the spin excitations spectrum. (b) Constant energy scans following the trajectory Q (1 0 l) with l = [0.4−0.6] at T = 6 K on the TAS 4F1. (c) Imaginary part of the dynamical magnetic susceptibility obtained by fits to the constant E scans.

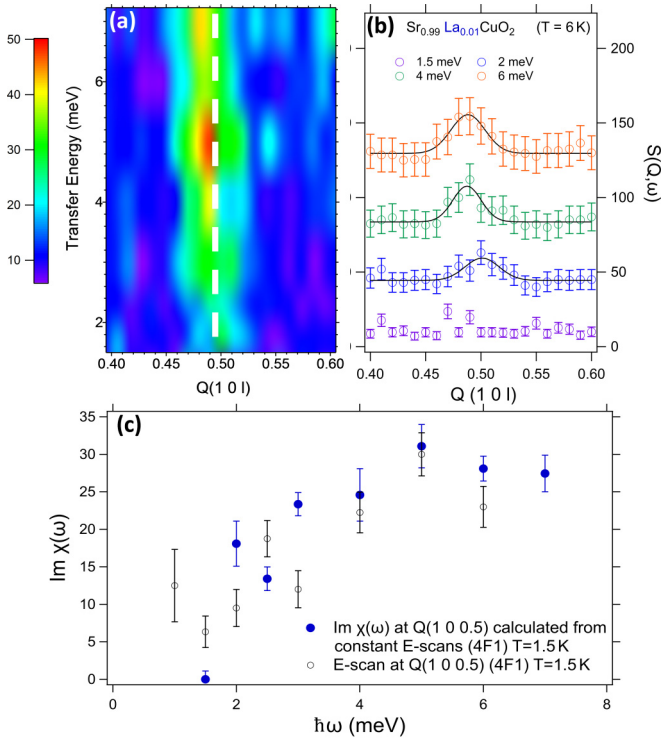

FIG. 9. (a) (Q, ω) color map of the low energy magnetic excitations spectrum obtained through INS in the La-doped $SrCuO_2$; the white dashed line shows the center of the spin excitations spectrum. (b) Constant energy scans following the trajectory Q (1 0 l) with l = [0.4−0.6] at T = 1.5 K on the TAS 4F1. (c) Comparison of the imaginary part of the dynamical magnetic susceptibility obtained by fits to the constant E scans and the energy scan at Q(1 0 0.5).

These results underline the fact that the system is purely 1D in $SrCuO_2$, as the two spinon continuum remains gapless and goes along with the fact that away from the magnetic ordering temperature, the ferromagnetic frustrated next nearest neighbor interaction in the zigzag chain (J_{FM}) remains weak compared to next neighbor interaction within the chain (J_{AFM}), resulting in a 1D system with only the single chain physical response.

2. Zn- and La-doped $SrCuO_2$

The constant energy scans obtained for the Zn- and La-doped $SrCuO_2$ are given in Fig. 8(b) and Fig. 9(b), respectively. The corresponding magnetic excitations spectra of the compounds are given in terms of Im (χ) in Fig. 8(c) and Fig. 9(c).

Measurements of the excitations spectra of the Zn- and La-doped compounds point out a strong decrease of the density of states in the low energy region of the spectra. This decay is already obvious from the (Q,ω) maps [Fig. 8(a) and Fig. 9(a)] for the Zn- and La-doped $SrCuO_2$, respectively, and can be seen from the evolution of the imaginary part of the dynamical magnetic susceptibility in function of the transfer energy [Fig. 8(c) and Fig. 9(c), respectively].

Both kinds of substitutions result in the opening of a spin pseudogap in the, basically, gapless two-spinon continuum of $SrCuO_2$.

[1] N. Hlubek, P. Ribeiro, R. Saint-Martin, A. Revcolevschi, G. Roth, G. Behr, B. Büchner, and C. Hess, Phys. Rev. B **81**, 020405 (2010).

[2] N. Hlubek, X. Zotos, S. Singh, R. Saint-Martin, A. Revcolevschi, B. Büchner, and C. Hess, J. Stat. Mech. Theory Exp. (2012) P03006.

[3] C. Hess, C. Baumann, U. Ammerahl, B. Büchner, F. Heidrich-Meisner, W. Brenig, and A. Revcolevschi, Phys. Rev. B **64**, 184305 (2001).

[4] A. V. Sologubenko, K. Giannò, H. R. Ott, A. Vietkine, and A. Revcolevschi, Phys. Rev. B **64**, 054412 (2001).

[5] Y. Matsushita, Y. Oyama, M. Hasegawa, and H. Takei, J. Solid State Chem. **114**, 289 (1995).
[6] M. Matsuda and K. Katsumata, J. Magn. Magn. Mater. **140**, 1671 (1995).
[7] H. Eisaki, N. Motoyama, and S. Uchida, Phys. C Supercond. **282**, 1323 (1997).
[8] R. Saint-Martin, P. Berthet, and A. Revcolevschi, J. Cryst. Growth **415**, 118 (2015).
[9] K. Karmakar, R. Bag, and S. Singh, Cryst. Growth Des. **15**, 4843 (2015).
[10] I. A. Zaliznyak, C. Broholm, M. Kibune, M. Nohara, and H. Takagi, Phys. Rev. Lett. **83**, 5370 (1999).
[11] M. Matsuda, K. Katsumata, K.M. Kojima, M. Larkin, G. M. Luke, J. Merrin, B. Nachumi, Y. J. Uemura, H. Eisaki, N. Motoyama, S. Uchida, and G. Shirane, Phys. Rev. B **55**, R11953 (1997).
[12] T. Ami, M. K. Crawford, R. L. Harlow, Z. R. Wang, D. C. Johnston, Q. Huang, and R. W. Erwin, Phys. Rev. B **51**, 5994 (1995).
[13] I. A. Zaliznyak, H. Woo, T. G. Perring, C. L. Broholm, C. D. Frost, and H. Takagi, Phys. Rev. Lett. **93**, 087202 (2004).
[14] T. Giamarchi, *Quantum Physics in One Dimension* (Clarendon Press, Oxford University, Oxford, 2003).
[15] A. M. Tsvelik, *Quantum Field Theory in Condensed Matter Physics* (Cambridge University Press, Cambridge, 2007).
[16] J. des Cloizeaux and J. J. Pearson, Phys. Rev. **128**, 2131 (1962).
[17] H. Bethe, Z. Für Phys. **71**, 205 (1931).
[18] G. Simutis, S. Gvasaliya, M. Mansson, A. L. Chernyshev, A. Mohan, S. Singh, C. Hess, A. T. Savici, A. I. Kolesnikov, A. Piovano, T. Perring, I. Zaliznyak, B. Büuchner, and A. Zheludev, Phys. Rev. Lett. **111**, 067204 (2013).
[19] K. Karmakar, R. Bag, M. Skoulatos, C. Rüegg, and S. Singh, arXiv:1706.01262 (2017).
[20] F. Hammerath, E. M. Brüning, S. Sanna, Y. Utz, N. S. Beesetty, R. Saint-Martin, A. Revcolevschi, C. Hess, B. Büchner, and H.-J. Grafe, Phys. Rev. B **89**, 184410 (2014).
[21] F. Hammerath, S. Nishimoto, H.-J. Grafe, A. U. B. Wolter, V. Kataev, P. Ribeiro, C. Hess, S.-L. Drechsler, and B. Büchner, Phys. Rev. Lett. **107**, 017203 (2011).
[22] G. Simutis, S. Gvasaliya, N. S. Beesetty, T. Yoshida, J. Robert, S. Petit, A. I. Kolesnikov, M. B. Stone, F. Bourdarot, H. C. Walker, D. T. Adroja, O. Sobolev, C. Hess, T. Masuda, A. Revcolevschi, B. Büchner, and A. Zheludev, Phys. Rev. B **95**, 054409 (2017).
[23] S. Eggert and I. Affleck, Phys. Rev. B **46**, 10866 (1992).
[24] J. C. Bonner and M. E. Fisher, Phys. Rev. **135**, A640 (1964).
[25] D. C. Johnston, R. K. Kremer, M. Troyer, X. Wang, A. Klümper, S. L. Bud'ko, A. F. Panchula, and P. C. Canfield, Phys. Rev. B **61**, 9558 (2000).
[26] G. Simutis, M. Thede, R. Saint-Martin, A. Mohan, C. Baines, Z. Guguchia, R. Khasanov, C. Hess, A. Revcolevschi, B. Büchner, and A. Zheludev, Phys. Rev. B **93**, 214430 (2016).
[27] S. Chattopadhyay, S. Giri, and S. Majumdar, J. Phys. Condens. Matter **23**, 216006 (2011).
[28] M. Matsuda, K. Katsumata, A. Zheludev, S. M. Shapiro, and G. Shirane, J. Phys. Chem. Solids **60**, 1121 (1999).
[29] G. Müller, H. Thomas, H. Beck, and J. C. Bonner, Phys. Rev. B **24**, 1429 (1981).
[30] V. Kataev, K.-Y. Choi, M. Grüninger, U. Ammerahl, B. Büchner, A. Freimuth, and A. Revcolevschi, Phys. Rev. B **64**, 104422 (2001).
[31] B. Lake, A. Tennant, C. Frost, and S. Nagler, Nat. Mater. **4**, 329 (2005).